



THE UNIVERSITY *of* EDINBURGH

Edinburgh Research Explorer

## Impact of surface physisorption on the gas scattering dynamics

**Citation for published version:**

Chen, Y, Gibelli, L, Li, J & Borg, MK 2023, 'Impact of surface physisorption on the gas scattering dynamics', *Journal of Fluid Mechanics*, vol. 968, A4. <https://doi.org/10.1017/jfm.2023.496>

**Digital Object Identifier (DOI):**

[10.1017/jfm.2023.496](https://doi.org/10.1017/jfm.2023.496)

**Link:**

[Link to publication record in Edinburgh Research Explorer](#)

**Document Version:**

Peer reviewed version

**Published In:**

Journal of Fluid Mechanics

**General rights**

Copyright for the publications made accessible via the Edinburgh Research Explorer is retained by the author(s) and / or other copyright owners and it is a condition of accessing these publications that users recognise and abide by the legal requirements associated with these rights.

**Take down policy**

The University of Edinburgh has made every reasonable effort to ensure that Edinburgh Research Explorer content complies with UK legislation. If you believe that the public display of this file breaches copyright please contact [openaccess@ed.ac.uk](mailto:openaccess@ed.ac.uk) providing details, and we will remove access to the work immediately and investigate your claim.



Banner appropriate to article type will appear here in typeset article

# 1 **Impact of surface physisorption on the gas** 2 **scattering dynamics**

3 **Yichong Chen<sup>1</sup>, Livio Gibelli<sup>1</sup>†, Jun Li<sup>2</sup> and Matthew K. Borg<sup>1</sup>‡**

4 <sup>1</sup>School of Engineering, University of Edinburgh, Edinburgh EH9 3FB, United Kingdom

5 <sup>2</sup>Center for Integrative Petroleum Research, College of Petroleum Engineering and Geosciences, King  
6 Fahd University of Petroleum and Minerals, Dhahran 31261, Saudi Arabia

7 (Received xx; revised xx; accepted xx)

8 Engineering flow systems operating under low pressures and/or at the micro/nano scale  
9 generally include a physically adsorbed gas layer next to the surface. In this paper, we  
10 develop a scattering kernel that accounts for the effect of adsorption, arising from van der  
11 Waals interactions, on the dynamics of molecules impinging on solid smooth surfaces. In  
12 the limit of low bulk density, surface adsorption becomes negligible and the scattering  
13 kernel recovers consistently the Cercignani-Lampis model, which best describes molecular  
14 collisions with a clean, smooth surface. In the limit of high bulk density, a dense adsorbed  
15 molecular layer forms next to the surface and its presence is picked up by the Maxwell model  
16 with complete diffuse reflection, which better captures the multiple collisions suffered by  
17 molecules. A weight coefficient based on the Langmuir adsorption isotherm is incorporated  
18 into the modelling to handle the transition between these two limiting conditions of low and  
19 high densities. The proposed model is validated against high-fidelity molecular dynamics  
20 simulations that are performed for a variety of gas-surface combinations and adsorbed  
21 molecular layers with different densities. It is shown that the proposed model very well  
22 captures the scattering patterns of beams of gas molecules at different velocities impinging  
23 on surfaces, as well as momentum and energy accommodation coefficients in the entire range  
24 of explored conditions.

25 **Key words:** (see [Keyword PDF](#) for the full list).

---

## 26 **1. Introduction**

27 When the condition of local quasi-thermodynamic equilibrium breaks down, dilute fluid  
28 flows are no longer governed by the Navier-Stokes equations with stick boundary conditions,  
29 and kinetic theory is required. The fluid behaviour must then be described by the Boltzmann  
30 equation, or a kinetic model equation, supplemented by boundary conditions that model the  
31 gas-surface interactions. These molecular interactions are typically formulated via the so-  
32 called scattering kernel (SK), which provides the probability density function of the molecules

† Email address for correspondence: livio.gibelli@ed.ac.uk

‡ Email address for correspondence: matthew.borg@ed.ac.uk

33 back-scattered into the gas after striking the surface. Typically, SKs contain a few parameters,  
34 referred to as accommodation coefficients (AC), which describe how some physical properties  
35 of the impinging molecular flux (e.g., momentum and energy) accommodate to the state of  
36 the surface. SKs are of paramount importance in non-equilibrium gas dynamics simulations  
37 because they determine the velocity slip and temperature jump at the surface, which are the  
38 macroscopic hallmarks of the fluid non-equilibrium conditions, and, in turn, affect the overall  
39 flow field increasingly with the gas rarefaction.

40 The most famous and extensively used SK was proposed by Maxwell (1879). The Maxwell  
41 model assumes that a fraction of incident gas molecules are diffusely reflected, while others  
42 are re-emitted specularly. Despite being widely used, the Maxwell model is unable to  
43 reproduce the lobular re-emission patterns that are experimentally observed when a nearly  
44 monoenergetic atomic beam hits the surface (Cercignani & Lampis 1971). Much effort has  
45 been employed over the years towards developing more accurate SKs that incorporate the  
46 gas-surface interactions.

47 Epstein (1967) extended the Maxwell model by replacing the constant accommodation  
48 coefficient with a function of the molecular velocity to reflect the dependency of the scattering  
49 dynamics on the velocity of the incident particle. Furthermore, Klinc & Kuščer (1972)  
50 considered the particular case of diffuse-elastic scattering, where molecules are isotropically  
51 back-scattered into the gas but conserve their impinging speed. A more general SK is the  
52 Cercignani-Lampis (CL) model (Cercignani & Lampis 1971; Cercignani 1972) that was  
53 derived by solving the half-space transport equation describing the dynamics of gas atoms  
54 within the wall modelled as a homogeneous and non-polar medium. It is worth stressing that  
55 the CL model was also obtained by using different approaches (Kuščer *et al.* 1971; Williams  
56 1971; Cowling 1974; Takata *et al.* 2021) and was proved to be the most general mathematical  
57 expression consistent with the basic properties that all SKs are expected to fulfil (see §2  
58 for more details of these basic kernel properties).

59 SKs have also been proposed that linearly combine the models above. Struchtrup (2013)  
60 combined the Maxwell model with the diffuse-elastic SK. The resulting model provides  
61 results similar to the CL model but has a simpler mathematical expression that makes it easier  
62 to derive boundary conditions for extended moment equations. In the Yamamoto-Takeuchi-  
63 Hyakutake (YTH) model (Yamamoto *et al.* 2007), it is assumed that a fraction of scattered  
64 molecules follow a CL-like model, while the remaining molecules are diffusely reflected.  
65 This model provides scattering patterns in better agreement with Molecular Dynamics (MD)  
66 simulations when the surface is contaminated with a fixed amount of heavy molecules  
67 while bombarded with lighter gas. However, the YTH model did not contain links with the  
68 contaminant information nor the adsorption physics. It is a phenomenological model where  
69 the AC functions are fitted from specific simulations conditions and are thus not general.  
70 The combination of Epstein and CL models was also proposed, and it was shown that it  
71 more accurately captures the trajectory of molecules in the scattering process (Yakunchikov  
72 *et al.* 2012), while providing an accurate description of both the Poiseuille and thermal  
73 transpiration flows (Wu & Struchtrup 2017).

74 Despite the many studies devoted to gas-surface interactions, relatively little attention has  
75 been paid to the development of SKs that incorporate adsorption (Kuščer 1978; Borman  
76 *et al.* 1988; Aoki & Giovangigli 2019, 2021; Aoki *et al.* 2022; Brancher *et al.* 2020).  
77 Yet, experimental, theoretical, and numerical evidence clearly indicates that neglecting  
78 the presence of adsorbed molecules oversimplifies the scattering dynamics and introduces  
79 inaccuracies in the resulting prediction of fluid flow. This was firstly highlighted in a  
80 pioneering experimental study, where it was shown that ACs of gases in contact with single-  
81 crystal silicon approach unity as pressure increases (Arkilic *et al.* 2001). Thereafter, this  
82 has been attributed to adsorption, as ACs have been found to significantly increase if the

83 surface gets adsorbed with gas molecules, reaching unity when a full adsorbed layer is formed  
 84 (Sazhin *et al.* 2001; Yamamoto *et al.* 2006; Finger *et al.* 2007; Chew 2009; Nejad *et al.* 2020).

85 A better understanding of how adsorption affects the scattering dynamics is not only of  
 86 theoretical interest, but also has relevant practical implications. Examples range from a more  
 87 accurate prediction of aerodynamic drag forces on satellites operating on very low Earth  
 88 orbits, where these forces are strongly dependent on the variation of the atomic-oxygen  
 89 adsorption with altitude (Pilinski *et al.* 2013; Livadiotti *et al.* 2020), to the enhancement  
 90 of the manufacturing throughput of microprocessor chips in low vacuum photolithography  
 91 machines, where adsorption of contaminants is detrimental (Chen 2005). More generally,  
 92 adsorption is expected to significantly affect the transport of nanoscale confined fluid  
 93 flows (Shan *et al.* 2022), such as hydrocarbons inside tight shale reservoirs (Wang *et al.*  
 94 2021), and the heat transfer efficiency in micro-electro-mechanical systems (MEMS) due to  
 95 the large surface-area-to-volume ratios characterising these problems (Cao *et al.* 2009).

96 This paper aims to derive a new SK that captures the effect of adsorption, arising from van  
 97 der Waals interactions only (also known in the literature as physisorption) on the scattering  
 98 dynamics, and unravel the resulting density-dependence on the ACs. The proposed kernel is  
 99 the linear combination of the CL model for a clean, smooth surface and the fully diffusive  
 100 Maxwell model for a surface covered by a dense gas layer, with the weight of the combination  
 101 proportional to the Langmuir adsorption isotherm (Langmuir 1916). The proposed kernel  
 102 is validated using high-fidelity MD simulations with Lennard-Jones (LJ) potentials that  
 103 accurately resolve the trajectories of molecules interacting with each other in the adsorbed  
 104 layer and with the surface.

105 It is important to emphasise that our study takes a different approach to model the  
 106 physics of adsorption than most past research. In particular, while we propose an SK to  
 107 capture the overall effects of adsorption, previous studies have attempted to derive models  
 108 from first principles. For example, Borman *et al.* (1988) proposed a kinetic equation to  
 109 study the dynamics of gas molecules in a potential field generated by surface atoms, with  
 110 molecule-phonon collisions accounting for fluctuations, and this approach has recently  
 111 been extended to include adsorption and chemical reactions on crystal surfaces (Aoki &  
 112 Giovangigli 2019, 2021; Aoki *et al.* 2022). Despite its ability to precisely capture the  
 113 intricate physics of adsorption, this kinetic equation-based modelling is computationally  
 114 demanding and not suitable for engineering simulations. On the other hand, our modelling  
 115 approach has similarities with the pioneering work of Kuščer (1978) and more recently  
 116 of Brancher *et al.* (2020). However, our focus is primarily on the case of a steady adsorbed  
 117 gas layer adjacent to the walls, whereas these two references mainly explore non-equilibrium  
 118 adsorption-desorption phenomena. A more in-depth comparative analysis of these studies is  
 119 presented in Section 3.

120 The remaining structure of this paper is as follows. The definition of SKs is outlined in  
 121 §2. The new SK, which encompasses the effect of adsorption, is derived in §3. The set-up  
 122 of high-fidelity MD simulations used in this work is presented in §4. In §5, an extensive  
 123 validation study is carried out to evaluate the scattering patterns and the ACs as functions of  
 124 the gas bulk density. Finally, concluding remarks are given in §6.

## 125 2. Scattering kernels and their accommodation coefficients

126 The scattering kernel  $\mathcal{R}(\xi' \rightarrow \xi; \mathbf{r}, t; \epsilon, \tau)$  gives the probability density that a molecule  
 127 striking the surface at position  $\mathbf{r} - \epsilon$  and time  $t - \tau$  with a velocity range of  $[\xi', \xi' + d\xi']$ ,  
 128 re-emerges away from the surface at position  $\mathbf{r}$  and time  $t$  with a velocity range of  $[\xi, \xi + d\xi]$ ,  
 129 where  $\epsilon$  is the distance travelled by the molecule in its adsorbed state and  $\tau$  is the adsorption

130 time (Cercignani 1988). The balance of mass at the surface yields:

$$131 \quad \xi_n f(\boldsymbol{\xi}, \mathbf{r}, t) = \int_{-\infty}^{\infty} d\boldsymbol{\epsilon} \int_0^{\infty} d\tau \int_{\xi'_n < 0} |\xi'_n| \mathcal{R}(\boldsymbol{\xi}' \rightarrow \boldsymbol{\xi}; \mathbf{r}, t; \boldsymbol{\epsilon}, \tau) f(\boldsymbol{\xi}', \mathbf{r} - \boldsymbol{\epsilon}, t - \tau) d\boldsymbol{\xi}', \quad (2.1)$$

132 where  $f(\boldsymbol{\xi}', \mathbf{r} - \boldsymbol{\epsilon}, t - \tau)$  and  $f(\boldsymbol{\xi}, \mathbf{r}, t)$  are the incident and reflected velocity distribution  
 133 functions, respectively, and the subscript  $n$  denotes the normal velocity component along  
 134 the unit vector normal to the surface pointing into the gas. If the gas-surface interactions  
 135 are dominated by physical van der Waals forces only, the adsorption time interval  $\tau$  and the  
 136 re-emission displacement  $\boldsymbol{\epsilon}$  are typically much smaller than the characteristic time and length  
 137 scales of the interactions between fluid molecules, and the SK simplifies to  $\mathcal{R}(\boldsymbol{\xi}' \rightarrow \boldsymbol{\xi})$ . This  
 138 condition is particularly valid for steady flow problems and is met in many situations of  
 139 practical importance, including the scattering from porous organic kerogen surfaces (Chen  
 140 *et al.* 2022).

141 SKs must satisfy the basic properties of

142 (i) Positiveness:

$$143 \quad \mathcal{R}(\boldsymbol{\xi}' \rightarrow \boldsymbol{\xi}) \geq 0, \quad (2.2)$$

144 (ii) Normalisation:

$$145 \quad \int_{\xi_n > 0} \mathcal{R}(\boldsymbol{\xi}' \rightarrow \boldsymbol{\xi}) d\boldsymbol{\xi} = 1, \quad (2.3)$$

146 if the surface is impermeable and permanent adsorption is excluded; and

147 (iii) Reciprocity:

$$148 \quad |\xi'_n| f_0(\boldsymbol{\xi}') \mathcal{R}(\boldsymbol{\xi}' \rightarrow \boldsymbol{\xi}) = |\xi_n| f_0(\boldsymbol{\xi}) \mathcal{R}(-\boldsymbol{\xi} \rightarrow -\boldsymbol{\xi}'), \quad (2.4)$$

149 where  $f_0(\boldsymbol{\xi})$  is the non-drifting Maxwellian distribution having the temperature of the wall.  
 150 The reciprocity indicates that microscopic scattering dynamics is time-reversible and the  
 151 surface is assumed to be in a local equilibrium state, undisturbed by the impinging molecules  
 152 (Kuščer 1971; Cercignani 1988). Specifically, the number of molecules scattered from a  
 153 velocity range  $[\boldsymbol{\xi}', \boldsymbol{\xi}' + d\boldsymbol{\xi}']$  to a velocity range  $[\boldsymbol{\xi}, \boldsymbol{\xi} + d\boldsymbol{\xi}]$  (per unit area and unit time)  
 154 is equal to the number of molecules scattered from any velocity within  $[-\boldsymbol{\xi}, -\boldsymbol{\xi} - d\boldsymbol{\xi}]$  to a  
 155 velocity within  $[-\boldsymbol{\xi}', -\boldsymbol{\xi}' - d\boldsymbol{\xi}']$ .

156 Cercignani (1988) proved that the simplest mathematical expression consistent with these  
 157 properties takes the general form:

$$158 \quad \mathcal{R}_G(\boldsymbol{\xi}' \rightarrow \boldsymbol{\xi}) = \mathcal{R}_{G,t}(\boldsymbol{\xi}'_t \rightarrow \boldsymbol{\xi}_t) \mathcal{R}_{G,n}(\xi'_n \rightarrow \xi_n), \quad (2.5a)$$

159 where

$$160 \quad \mathcal{R}_{G,t}(\boldsymbol{\xi}'_t \rightarrow \boldsymbol{\xi}_t) = \frac{(1 - q^2)^{-1}}{2\pi RT_0} \exp\left\{-\frac{1}{1 - q^2} \frac{(\boldsymbol{\xi}_t - q\boldsymbol{\xi}'_t)^2}{2RT_0}\right\}, \quad q \in [-1, 1], \quad (2.5b)$$

$$161 \quad \mathcal{R}_{G,n}(\xi'_n \rightarrow \xi_n) = \frac{(1 - p)^{-1} \xi_n}{RT_0} \exp\left\{-\frac{\xi_n^2 + p\xi_n'^2}{2RT_0(1 - p)}\right\} I_0\left(\frac{\sqrt{p}}{1 - p} \frac{\xi_n \xi'_n}{RT_0}\right), \quad p \in [0, 1], \quad (2.5c)$$

162  
 163  
 164  $\boldsymbol{\xi}_t$  is the two dimensional vector lying on the surface with velocity components  $\xi_{t1}$  and  $\xi_{t2}$  (for  
 165 an isotropic surface, the scattering dynamics of  $\xi_{t1}$  and  $\xi_{t2}$  are equivalent),  $R$  is the specific  
 166 gas constant,  $T_0$  is the wall temperature, and  $I_0$  is the modified Bessel function of the first  
 167 kind and zeroth order.

168 The parameters  $p$  and  $q$  can be related to the so-called ACs that possess a more transparent

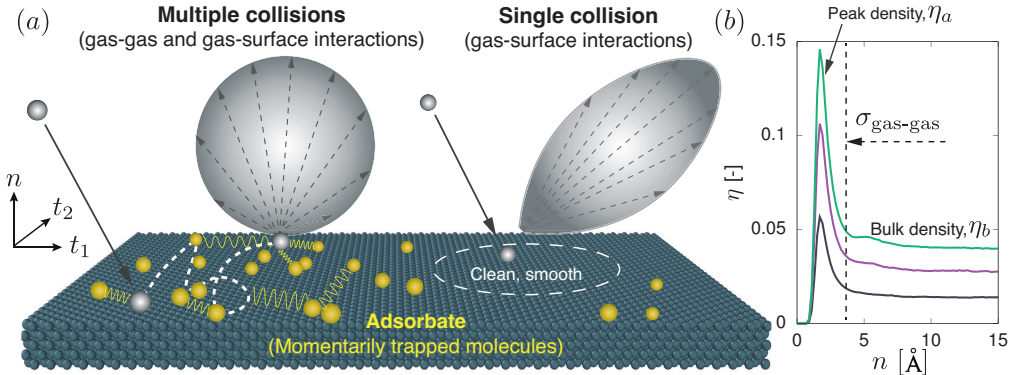


Figure 1: (a) Schematic of scattering dynamics of gas molecules near a smooth surface. During the scattering process, incident gas molecules (grey) could either suffer single or multiple collisions (both with the wall and other momentarily adsorbed gas molecules). (b) Example density profiles in the presence of argon (Ar) molecules near the platinum (Pt) surface at an equilibrium temperature of 300 K, with distinguishable features of bulk and elevated adsorption densities.

169 physical meaning. These give the tendency of the gas property associated with a specified  
 170 molecular velocity function  $\varphi(\xi)$  to accommodate to the state of the wall. The general ACs  
 171 are typically defined as (Kuščer 1974; Cercignani 1988; Sharipov 2002):

$$172 \quad \alpha(\varphi) = \frac{\int_{\xi'_n < 0} \varphi(\xi') |\xi'_n| f(\xi') d\xi' - \int_{\xi_n > 0} \varphi(\xi) |\xi_n| f(\xi) d\xi}{\int_{\xi'_n < 0} \varphi(\xi') |\xi'_n| f(\xi') d\xi' - \int_{\xi_n > 0} \varphi(\xi) |\xi_n| f_0(\xi) d\xi}, \quad (2.6)$$

173 where  $f_0(\xi)$  is the wall Maxwellian velocity distribution function. As an example, by  
 174 setting  $\varphi(\xi) = \xi_t$ ,  $\xi_n^2/2$ ,  $\xi^2/2$ , the accommodation coefficients for the tangential momentum  
 175 (TMAC,  $\alpha_t$ ), normal kinetic energy (NEAC,  $\alpha_{E_n}$ ), and kinetic energy (EAC,  $\alpha_E$ ) are obtained.  
 176 Note that beam ACs  $\alpha^b(\varphi)$  are also used that correspond to the cases of monoenergetic  
 177 impinging beams (Kuščer 1974), i.e.,  $f(\xi') = n_b \delta(\xi' - \xi_b)$  with  $n_b$  being the density of the  
 178 beam and  $\xi_b$  a fixed velocity.

179 It is worth stressing that the definition of the accommodation coefficients, (2.6), has two  
 180 shortcomings. First, for an SK in the form of (2.5), only TMAC and NEAC are independent  
 181 of the impinging velocity distribution (Cercignani 1988). Second, when the system is close  
 182 to the equilibrium state, i.e.,  $f(\xi') \approx f(\xi) \approx f_0(\xi)$ , both numerator and denominator in  
 183 (2.6) approach zero and numerical inaccuracies arise, which require specific procedures to  
 184 cope with these instances (Kuščer 1974; Cercignani 1988; Spijker *et al.* 2010).

185 All the existing SKs can readily be obtained by the general form of (2.5) (or by linearly  
 186 combining expressions of this form) along with ACs, e.g.,

$$187 \quad \text{Maxwell model:} \quad q_1 = 0, \quad q_2 = 1, \quad p_1 = 0, \quad p_2 = 1, \quad (2.7a)$$

$$188 \quad \text{Cercignani-Lampis model:} \quad q = 1 - \alpha_t, \quad p = 1 - \alpha_{E_n}, \quad (2.7b)$$

$$189 \quad \text{YTH model:} \quad q_1 = 0, \quad q_2 = (1 - \alpha_t^b)^{1/2}, \quad p_1 = 0, \quad p_2 \approx 1 - \alpha_{E_n}^b. \quad (2.7c)$$

190

### 191 3. A new scattering dynamics model: incorporating adsorption

192 We present a new scattering model that incorporates the effect of gas adsorption on smooth  
 193 surfaces. Note the SK model we propose here is applicable to standard temperatures or



194 higher, so that quantum effects (Goodman & Wachman 1976*b*; Bird 1994*b*) do not play a  
 195 role and the classical scattering description is applicable. For simplicity, the effect of wall  
 196 roughness is omitted from this work.

197 Molecules impinging on smooth solid surfaces may be divided into two groups. The first  
 198 group comprises adsorbed molecules, namely molecules that are momentarily trapped and  
 199 suffer multiple collisions with the surface and/or other fluid molecules before moving away,  
 200 and as a result, are more likely to accommodate thermally with the surface (Kuščer 1978;  
 201 Rettner *et al.* 1989; Bird 1994*a*; Butt *et al.* 2003; Arya *et al.* 2003; Myong 2004; Cao *et al.*  
 202 2005). The second group is composed of molecules that, after hitting the clean part of the  
 203 surface (i.e., where no adsorption occurs locally), are immediately reflected back to the bulk  
 204 of the gas, and their behaviour is only expected to depend on the local microscopic features  
 205 of the surface. The scattering dynamics of these two groups are very different, as depicted in  
 206 the schematic of figure 1(a), and the rate of these contributions depends on the bulk density.  
 207 In the limit of high gas bulk density, the first scattering group dominates, while the second  
 208 scattering group is seen more in the limit of low gas bulk density.

209 Our SK is therefore a linear combination of these two limiting scattering contributions,  
 210 namely the fully-diffuse Maxwell model,  $\mathcal{R}_d$ , which properly captures the effect of multiple  
 211 collisions suffered with adsorbed molecules (often seen in the limit of high density), and the  
 212 CL model,  $\mathcal{R}_{CL}$ , which is deemed to provide the most accurate description of the interactions  
 213 of molecules with a clean, smooth surface (often seen in the limit of low density):

$$214 \quad \mathcal{R}_{\text{new},t} = \theta_1(\eta_b)\mathcal{R}_{d,t} + [1 - \theta_1(\eta_b)]\mathcal{R}_{CL,t}(\alpha_{t,0}), \quad (3.1a)$$

$$215 \quad \mathcal{R}_{\text{new},n} = \theta_2(\eta_b)\mathcal{R}_{d,n} + [1 - \theta_2(\eta_b)]\mathcal{R}_{CL,n}(\alpha_{E_n,0}), \quad (3.1b)$$

217 where  $\alpha_{t,0}$  and  $\alpha_{E_n,0}$  are the TMAC and NEAC of a smooth surface being free of adsorption,  
 218 and are called the intrinsic coefficients. In principle, these coefficients can be obtained either  
 219 from beam experiments performed in low vacuum systems (Goodman & Wachman 1976*a*),  
 220 or using approximate theoretical models (Goodman 1974). It is worth stressing that, from the  
 221 derivation of the CL model, the details of a collision between a gas molecule and a solid atom  
 222 (i.e., hard collisions) are assumed to be negligible, compared to the effect of simultaneously  
 223 grazing collisions (Cercignani 1988). Therefore, the accuracy of the CL model may decrease  
 224 when a corrugation effect exists from the crystal structure, as would be the case in the MD  
 225 simulations, which may contain a subtle corrugation in the gas-surface potential energy  
 226 landscape.

227 In (3.1), the function  $\theta_1$  represents the probability that a molecule striking the surface  
 228 behaves as an adsorbed molecule in the tangential component, and it is anticipated to be an  
 229 increasing function of the reduced bulk number density  $\eta_b = n_{\text{bulk}}\pi\sigma_{\text{gas-gas}}^3/6$ , where  $n_{\text{bulk}}$   
 230 is the bulk number density,  $\sigma_{\text{gas-gas}}$  is the diameter of a gas molecule; the function  $\theta_2$  has a  
 231 similar meaning, although for the normal component, but must be treated separately because  
 232 the tangential component is known to exhibit a faster accommodation rate to the state of the  
 233 surface than the normal one (Cercignani 1988; Chen *et al.* 2022).

234 The function  $\theta_1$  can be naturally related to the gas/surface coverage, defined as the ratio  
 235 between the occupied sites and the maximum binding sites available on the surface. Indeed,  
 236 the denser the adsorbed gas layer (i.e., the higher the peak density  $\eta_a$  shown in figure 1(b)) next  
 237 to the surface is, the higher becomes the probability that the gas molecule accommodates to  
 238 the state of the surface. The surface coverage can be predicted based on the classical Langmuir  
 239 adsorption isotherm (Langmuir 1916) when a monolayer adsorption forms adjacent to the  
 240 surface (see figure 1(b) for example density profiles). As for the function  $\theta_2$ , the simplest direct  
 241 proportionality relation is presumed also to exist with the surface coverage. Accordingly, in

242 dimensionless units, the combination coefficients read:

$$243 \quad \theta_1 = \frac{\hat{K}_L \eta_b}{1 + \hat{K}_L \eta_b}, \quad \theta_2 = C \frac{\hat{K}_L \eta_b}{1 + \hat{K}_L \eta_b}, \quad (3.2)$$

244 where  $C \in [0, 1]$  is a fitting constant, and  $\hat{K}_L$  is the Langmuir constant. It is worth  
 245 stressing that the Langmuir adsorption isotherm has already been used by Goodman  
 246 (1974) and Pilinski *et al.* (2013) for assessing the effect of adsorption on the energy and  
 247 thermal accommodation coefficients, and it is chosen here for its simplicity. However, in  
 248 principle, more sophisticated isotherm models can also be used, such as the Freundlich  
 249 model (Freundlich 1922) for heterogeneous surfaces and the Brunauer-Emmett-Teller (BET)  
 250 model for multilayer adsorption (Brunauer *et al.* 1938).

251 Note that, according to (3.1), the TMAC and NEAC of the new SK read:

$$252 \quad \alpha_t = \theta_1 + (1 - \theta_1) \alpha_{t,0}, \quad (3.3a)$$

$$253 \quad \alpha_{E_n} = \theta_2 + (1 - \theta_2) \alpha_{E_n,0}. \quad (3.3b)$$

255 As expected, the ACs recover their intrinsic values for clean, smooth surfaces, i.e.,  $\alpha_t \rightarrow$   
 256  $\alpha_{t,0}$ ,  $\alpha_{E_n} \rightarrow \alpha_{E_n,0}$  in the limit when  $\theta_1$  and  $\theta_2$  go to zero.

257 It is worth noting that Brancher *et al.* (2020) have proposed an SK with many similarities  
 258 to ours, namely a linear combination of Maxwell fully-diffuse and CL (or Maxwell with  
 259 incomplete accommodation). Unlike our model, which focuses solely on the effect of an  
 260 adsorbed gas layer in dynamic equilibrium, this model can explain the time variation of the  
 261 adsorbed surface coverage, which simplifies to the Langmuir isotherm when the adsorption  
 262 and desorption rates are in balance. However, the assumptions on the scattering dynamics  
 263 underlying this model differ from our model, as can be clearly seen by considering the two  
 264 limiting cases of clean and fully adsorbed surfaces. In particular, in the case of clean surfaces,  
 265 our SK simplifies to CL, while that of Brancher *et al.* (2020) remains a linear combination  
 266 of Maxwell fully-diffuse and CL, where the coefficient of the combination is the adsorption  
 267 probability. In the case of fully adsorbed surfaces, our SK simplifies to Maxwell fully-diffuse,  
 268 while that of Brancher *et al.* (2020) simplifies to the CL model. As discussed in detail in the  
 269 next section, our different modelling choices allow us to obtain scattering patterns in overall  
 270 good agreement with those predicted by MD.

#### 271 4. Modelling the scattering using molecular dynamics

272 In this work, the scattering dynamics of gas molecules is simulated by the molecular dynamics  
 273 (MD) method using the LAMMPS software (Plimpton 1995). By numerically integrating  
 274 Newton's equations of motion, MD is able to deterministically resolve the trajectories of gas  
 275 molecules interacting with the surface atoms.

276 In our simulations, surface atoms are constructed in a Face-Centred Cubic (FCC) arrange-  
 277 ment with a lattice parameter 3.92 Å, as shown in figure 1(a), and gas molecules are modelled  
 278 as monatomic for simplicity. It is worth stressing that very heavy gas molecules with high  
 279 intermolecular attraction, such as xenon, shall not be considered, as they could 'permanently'  
 280 stick to the surface, which violates the assumption of negligible residence time. To extend  
 281 the validation of scattering models from moderately heavy to light gas molecules, and  
 282 keep the gas-surface interaction unreactive, two distinct groups of gas-surface combinations  
 283 have been considered: argon-platinum (Ar-Pt) and helium-gold (He-Au), respectively. Each  
 284 combination has been investigated under various reduced bulk gas densities  $\eta_b$ , thereby  
 285 permitting one to consider adsorption of different degrees. The velocity-Verlet algorithm is  
 286 implemented for the trajectory integration with a time step of 1 fs, and interactions among



---

Argon-Platinum			Helium-Gold		
Atom pairs	$\sigma$ [Å]	$\epsilon/k$ [K]	Atom pairs	$\sigma$ [Å]	$\epsilon/k$ [K]
Ar-Ar	3.405	119.80	He-He	2.64	10.890
Pt-Pt	2.471	8053.6	Au-Au	2.630	2662.1
Ar-Pt	2.940	79.139	He-Au	4.342	9.1355

---

Table 1: Interatomic Lennard-Jones potential parameters ( $\sigma$ ,  $\epsilon$ ) used in the MD simulations. Molecular masses  $m$  [u]: Ar = 39.948; He = 4.0026; Pt = 195.084; Au = 196.967.

---

287 atoms are described by the standard 12-6 Lennard-Jones (LJ) potential:

$$288 \quad U_{\text{LJ}}(r) = 4\epsilon \left[ \left( \frac{\sigma}{r} \right)^{12} - \left( \frac{\sigma}{r} \right)^6 \right], \quad (4.1)$$

289 where  $r$  is the distance between pairs of atoms,  $\epsilon$  is the interatomic potential well depth,  
 290 and  $\sigma$  is the distance where the potential is zero. The interactions parameters for Ar-Pt and  
 291 He-Au, which are obtained from Spijker *et al.* (2010) and Liao *et al.* (2018), respectively, are  
 292 listed in table 1 with a LJ cut-off distance  $r = r_c = 15$  Å.

293 Each MD simulation run is divided into two steps: equilibration and production. During  
 294 equilibration, both gas molecules and wall atoms are kept at a constant temperature, using  
 295 the Nosé–Hoover thermostat, with a time constant of 100 fs in the NVT ensemble. Here, two  
 296 temperatures are considered: 300 K, for typical room temperature of MEMS devices, and  
 297 423 K, which we considered in an earlier scattering study (Chen *et al.* 2022), and is used  
 298 here as a test of an elevated temperature condition on our scattering model. Each parallel  
 299 wall has an outer edge of rigid wall molecules, which prevents any movement of the wall.  
 300 Following equilibration, the thermostat on the gas molecules is switched off such that their  
 301 scattering dynamics are not biased. The production run provides access to all Lagrangian  
 302 information from which the scattering data of interest can be calculated. Our scattering  
 303 results are recorded by placing an artificial virtual plane at a distance  $r_c$  away from, and  
 304 parallel to the surface, within which a gas molecule and a wall atom can still feel each other.  
 305 When a molecule from the bulk crosses the virtual plane, its incident information (e.g.,  
 306  $\xi', \mathbf{r} - \boldsymbol{\epsilon}, t - \tau$ ) is recorded. The reflected information of the same molecule will be recorded  
 307 again (e.g.,  $\xi, \mathbf{r}, t$ ) when it crosses the plane back into the bulk, as illustrated in figure 2(a)  
 308 (inset). Furthermore, the collisions of gas molecules within the near wall region can be  
 309 tracked. To accurately describe the scattering behaviour and construct the scattering function  
 310  $\mathcal{R}(\xi' \rightarrow \xi)$ , collisions  $O(10^6)$  are generally required, which leads to  $O(10^{-9})$  seconds of a  
 311 production run, depending on the dimension and density of the system. Further details of the  
 312 technique for measuring molecule scattering information can be found in Chen *et al.* (2022).  
 313

## 314 5. Results and validation

315 In this section, we first assess the accuracy of the assumptions underpinning our model  
 316 (§5.1). Afterwards, we calibrate the parameters of the proposed SK to best fit the MD results  
 317 for TMAC and NEAC in the range of gas bulk densities explored in this work (§5.2). Finally,  
 318 we show that the proposed SK well describes the interplay between momentum and energy  
 319 accommodation coefficients (§5.3.1), and more accurately predicts the scattering patterns

320 of monoenergetic beams (§5.3.2) provided by the MD simulations for different gas bulk  
321 densities and gas-surface systems.

### 322 5.1. Assessment of model assumptions

323 Our proposed SK relies on three key modelling assumptions. First, the higher the density  
324 of the adsorbed gas layer, the higher becomes the fraction of molecules suffering multiple  
325 collisions (assumption 1). Second, molecules suffering multiple collisions are more likely  
326 to accommodate to the state of the surface, where the rate of accommodation of the normal  
327 component is slower than the tangential one (assumption 2). Third, the fraction of molecules  
328 that are completely accommodated to the state of the surface can be identified with the  
329 surface coverage as given by the Langmuir isotherm (assumption 3). In the following, these  
330 assumptions will be assessed for the Ar-Pt system at temperature 423 K. However, similar  
331 qualitative trends were found for all systems carried out in this work, which are not reported  
332 here for brevity.

333 Assumptions 1 and 2 are examined in figure 2(a), which shows the probability histogram  
334 of the individual gas collisions that occur between the virtual plane and the wall; a collision  
335 occurs when a molecule’s velocity component changes sign, which captures both gas-gas  
336 and gas-surface collisions. It is apparent that when the surface is clean ( $\eta_a = \eta_b = 0$ ), a  
337 gas molecule has the highest probability of colliding only once, whereas the probability of  
338 multiple collisions increases with the density of the gas layer, as indicated by the larger tail  
339 of the histogram for larger  $\eta_b$ . Furthermore, figure 2(b) and (c) support assumption 2 by  
340 showing that molecules accommodate more strongly to the state of the surface if they collide  
341 multiple times (i.e., the ACs approach unity with higher number of collisions, where here the  
342 ACs refer to beams composed of molecules grouped based on the number of collisions they  
343 suffered), and the accommodation rate is faster for TMAC than for NEAC. It is worth noticing  
344 that TMAC shows a zig-zag-like behaviour. From a qualitative standpoint, we can explain  
345 this phenomenon using the illustration in figure 2(d) of some sample collisions: the number  
346 of changes in the tangential velocity component, denoted by  $N_t$ , occur more frequently on  
347 even collisions (e.g.  $N = 2, 4, \dots$ ) and this increases the rate of accommodation, leading to  
348 the higher TMACs observed in figure 2(b). The same argument explains why the behaviour  
349 of the NEAC is instead almost monotonic.

350 Assumption 3 is examined in figures 2(e) and (f). Molecules were first grouped in two  
351 categories depending on whether they collided twice (solid green symbols) or more than  
352 twice (solid black symbols) with the surface, and the TMAC of each group is computed  
353 as a function of the reduced bulk density. As shown in figure 2(e), the TMACs of the two  
354 groups follow trends that qualitatively match those of the solid lines that represent the two  
355 contributions featuring in the proposed SK, i.e.,  $\theta_1$  and  $(1 - \theta_1)\alpha_{t,0}$ , respectively (these  
356 contributions were computed using the model calibrated as discussed in §5.2). In figure 2(f)  
357 a similar comparison is presented for NEAC. However, the criterion used here to define the  
358 two groups is slightly different; namely, a higher collision threshold was considered (four  
359 collisions instead of two) to account for the expected lower accommodation rate of the normal  
360 velocity component compared to the tangential one. A good qualitative agreement is seen in  
361 this case as well.

### 362 5.2. Model calibration

363 The proposed SK features two groups of parameters, namely  $(\alpha_{t,0}, \alpha_{E_n,0})$ , which describe  
364 the re-emission dynamics from a clean, smooth surface, and  $(\hat{K}_L, C)$ , which account for the  
365 effects of the adsorbed gas layer. The first group of parameters was evaluated by computing  
366 TMAC and NEAC based on MD simulations in which gas-gas interactions are switched

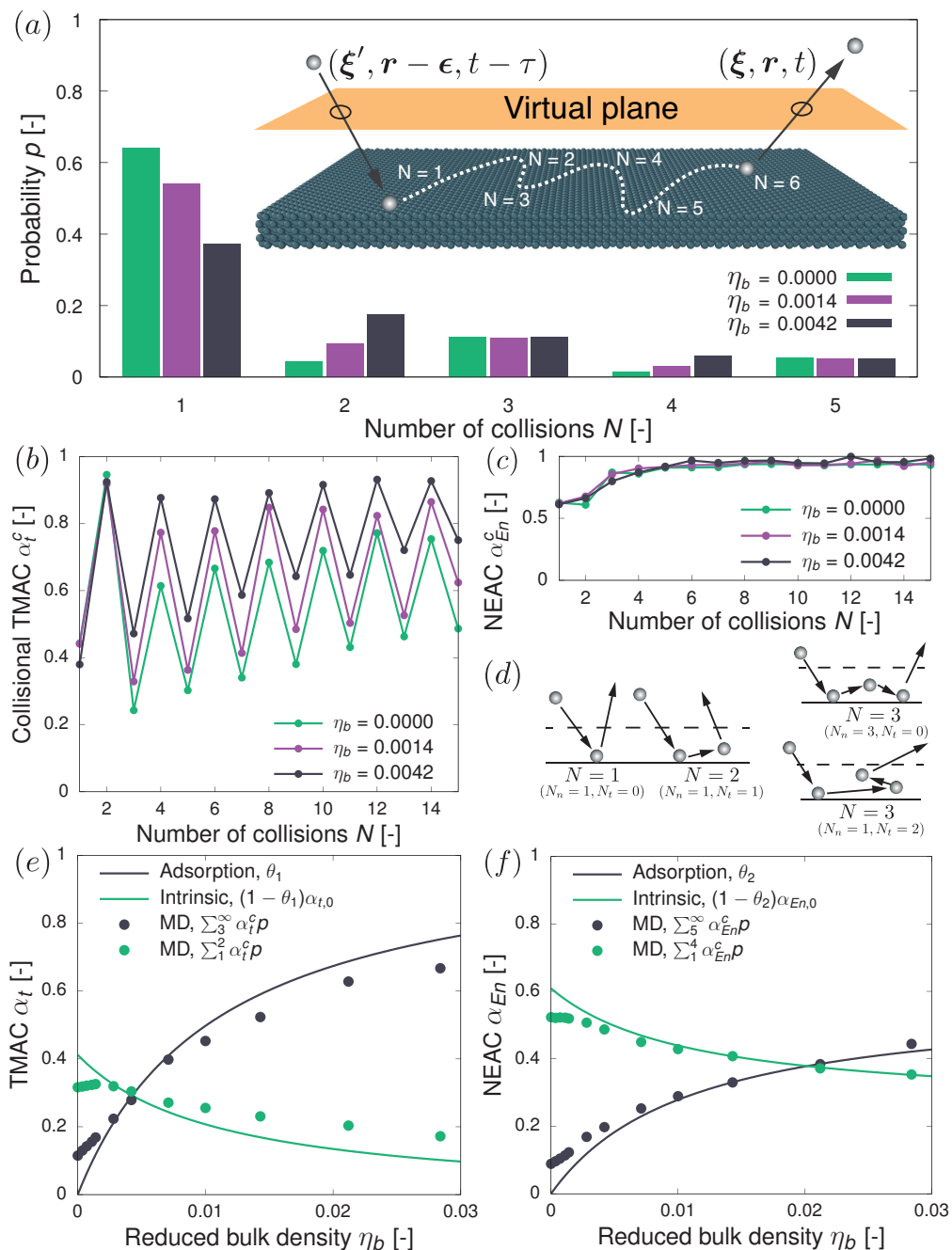


Figure 2: Scattering process of argon molecules on a platinum surface at 423 K. (a) Probability histogram of the number of collisions, with the inset indicating the tracking of the scattering process. (b) TMAC versus number of collisions. (c) NEAC versus number of collisions. (d) Qualitative schematics of odd versus even collisions. Contributions to (e) TMAC and (f) NEAC of molecules suffering two, for TMAC, and up to four, for NEAC, collisions (green colour) and multiple collisions (black colour) as functions of the reduced bulk density. Solid symbols are MD results and solid lines are the predictions of our calibrated SK, (3.3).

	$\alpha_{t,0}$		$\alpha_{E_n,0}$		$\hat{K}_L$		$C$	
	300 K	423 K	300 K	423 K	300 K	423 K	300 K	423 K
Ar-Pt	0.49	0.41	0.64	0.61	125.15	95.34	0.58	0.57
He-Au	0.07	0.11	0.14	0.18	102.59	90.36	0.69	0.73

Table 2: Reference values for the intrinsic accommodation coefficients ( $\alpha_{t,0}, \alpha_{E_n,0}$ ) and the calibrated constants ( $\hat{K}_L, C$ ).

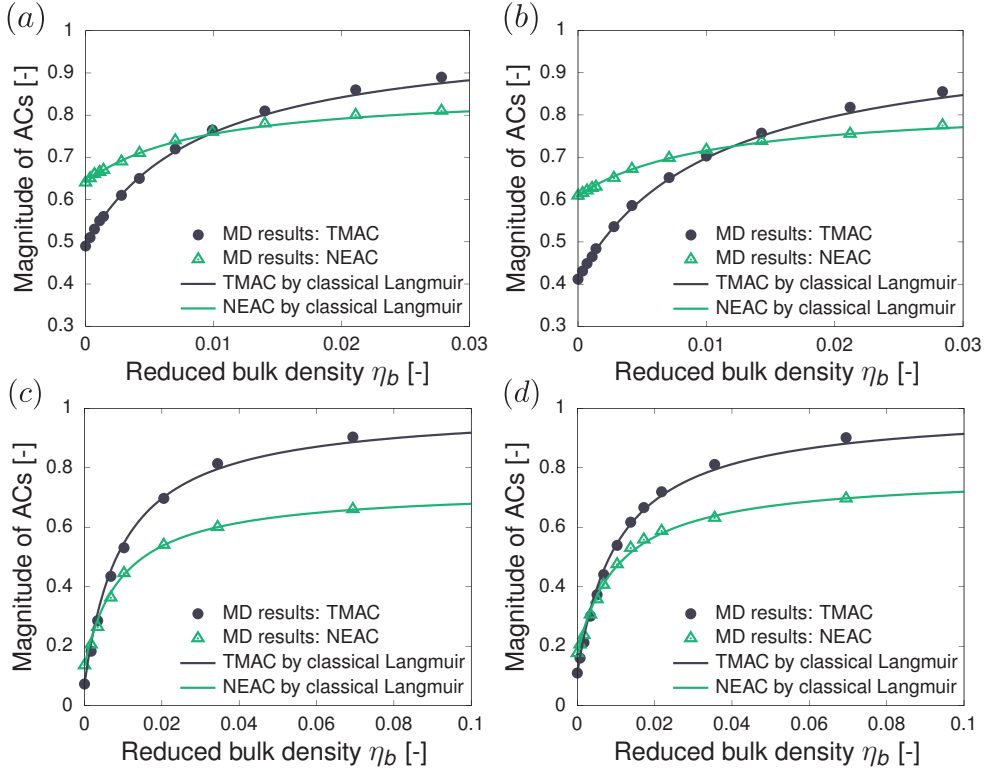


Figure 3: Variation of the general accommodation coefficients with bulk densities  $\eta_b$  given by MD results for the Ar-Pt system at (a) 300 K and (b) 423 K; the He-Au system at (c) 300 K and (d) 423 K.

367 off. Afterwards, the second group of parameters were calibrated by fitting (3.3), alongside  
368 (3.2), to the values of TMAC and NEAC corresponding to different reduced bulk densities  
369 provided by MD simulations, which include gas-gas interactions. Here, the two groups of  
370 parameters, obtained from our considered systems, are listed in table 2 for reference. The  
371 AC results measured from the MD are shown in figure 3 for the sample cases of Ar-Pt and  
372 He-Au systems at two different temperatures (solid symbols), along with the fitting curves  
373 (solid lines). An excellent agreement is found except for the larger values of the reduced bulk  
374 density, e.g., at  $T = 300$  K, deviations are less than 4% for the Ar-Pt system, and reduce to  
375 2% for the He-Au system. These deviations can be explained by the inability of the Langmuir  
376 isotherm to capture the interactions between adsorbed gas molecules that arise when a high-  
377 density gas layer covers the surface. However, by including the effect of repulsive lateral

---

Model	Intrinsic correlations
Maxwell	$\alpha_{E_t} = \alpha_t$
Cercignani-Lampis	$\alpha_{E_t} = \alpha_t(2 - \alpha_t)$
YTH	$\alpha_{E_t} = 1 - (1 - \alpha_t)^{3/2}$
Our proposed model (3.1)	$\alpha_{E_t} = \alpha_{t,0}(1 - \alpha_t) + \alpha_t$

---

Table 3: The relation between the TMAC ( $\alpha_t$ ) and the TEAC ( $\alpha_{E_t}$ ) for various SKs.

378 interactions on the adsorption and desorption rates (Butt *et al.* 2003), we verified that all MD  
379 data can be fitted within an accuracy of 3%.

380 Two remarks are worth making about the results reported in figure 3. First, the slope of  
381 NEAC is smaller than that of TMAC regardless of the temperature and gas-solid combination.  
382 This clearly highlights the slower accommodation of the energy to the state of the surface  
383 and, therefore, the need to introduce the constant  $C$  in (3.2). Second, the general ACs take  
384 smaller values as the temperature increases for the Ar-Pt system, while the opposite has been  
385 observed for the He-Au system.

### 386 5.3. Assessment of model predictivity

#### 387 5.3.1. Correlation between accommodation coefficients

388 The fundamental aspects of gas-surface interactions are fully encompassed in the SK, but  
389 ACs are also useful in that they provide some coarse-grained information about the dynamics  
390 of molecules impinging on the surface. As the SKs represented by (2.5) only contain one  
391 disposable parameter in the tangential component and another one in the normal component,  
392 relations must exist between ACs of quantities defined along the same directions. The relations  
393 between TMACs and tangential kinetic energy accommodation coefficients (TEACs) of the  
394 SKs considered in this study are listed in table 3, whereas those between normal momentum  
395 accommodation coefficients (NMACs) and NEACs were determined numerically because the  
396 presence of the Bessel function prevents one to easily obtain results in closed form. Note that  
397 the relations between TMACs and TEACs do not depend on the impingement distribution  
398 but this is not the case for the relations between NMACs and NEACs. The results presented  
399 in this section refer to a Maxwellian impingement that typically occurs when considering  
400 low-speed gas flows.

401 Figure 4 shows the relations between TMAC and TEAC (panel (a)) and between NMAC  
402 and NEAC (panel (b)) provided by MD simulations for various reduced densities (solid  
403 symbols), along with the predictions of the SKs (solid lines). It is apparent that the proposed  
404 SK provides the best match with MD results in the range of explored reduced densities. The  
405 predictions of the Maxwell model are in poor agreement with MD results, especially for the  
406 smaller values of  $\eta_b$ . The CL model agrees reasonably well with our MD results in this limit,  
407 whereas large discrepancies of the CL model can be clearly seen in figure 4(a) when the  
408 surface adsorption increases. The YTH model shows an agreement at intermediate densities.  
409 Note here we carry out the same phenomenological fit for the YTH model with our MD  
410 simulations, using the general accommodation coefficients.

#### 411 5.3.2. Scattering patterns

412 A more accurate assessment of the SKs is here carried out by comparing the scattering  
413 patterns of monoenergetic beams provided by each model against MD simulation results. In  
414 these numerical experiments, a monoenergetic beam is obtained by selecting only those

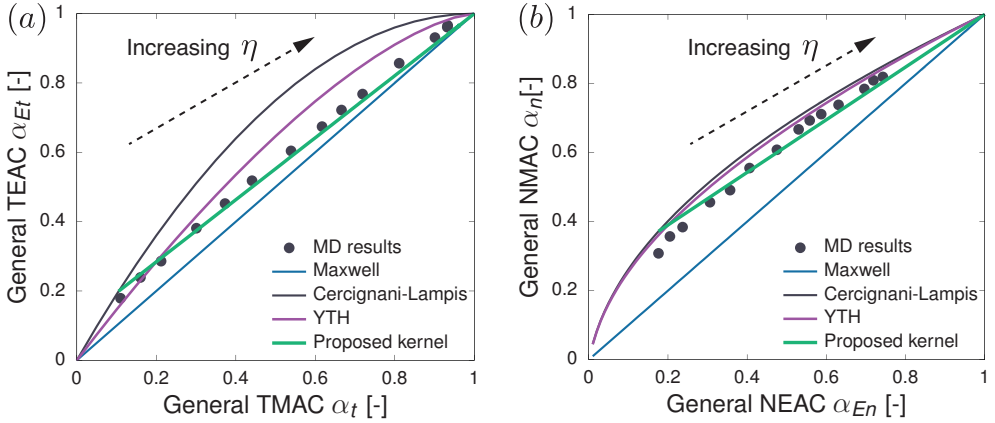


Figure 4: The relation between momentum and energy accommodation coefficients for the He-Au system at 423 K, given by our MD results and predicted by various SKs. (a) TEAC versus TMAC; (b) NMAC versus NEAC. Density of data points correspond to those in figure 3(d).

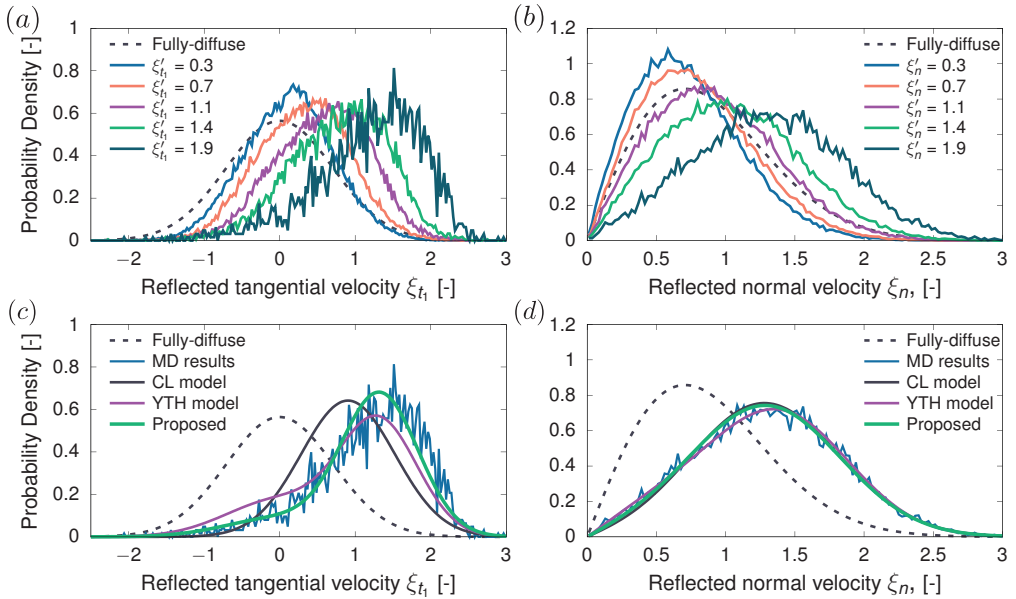


Figure 5: Re-emission probability distributions of the (a) tangential and (b) normal velocity for monoenergetic beams predicted by MD for Ar-Pt system with surface temperature 423 K and  $\eta_b = 0.0011$ . Velocities of the beams are normalised by the most probable speed  $\sqrt{2RT}$ . In (c)-(d) MD results are compared against predictions of the SKs for an example of high impinging velocity of  $\xi'_{t_1} = 1.9$  and  $\xi'_{n_1} = 1.9$ .

415 molecules bombarding the surface which have their tangential (normal) component of  
 416 velocity in the range  $[\xi', \xi' + \Delta\xi']$ , and re-emission probabilities of the velocity components  
 417 are evaluated accordingly.

418 Figures 5(a-b) show the reflected velocity distributions of argon molecules scattered from  
 419 a platinum surface at 423 K. An example value of the reduced bulk density is presented  
 420 here, i.e.,  $\eta_b = 0.0011$ , to highlight the different predictions of the SKs, since in the limiting



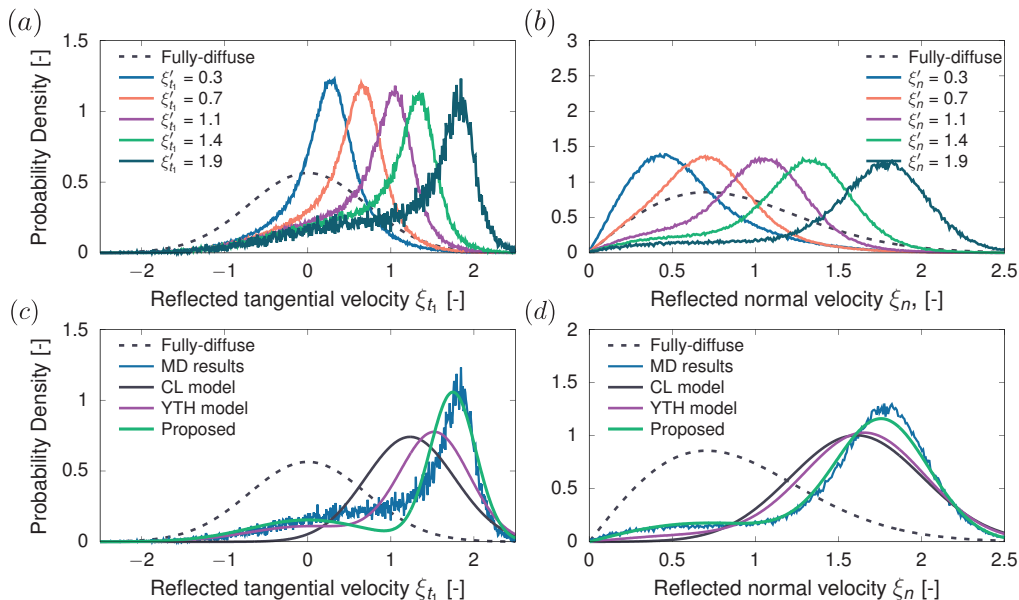


Figure 6: Re-emission probability distributions of the (a) tangential and (b) normal velocity for monoenergetic beams predicted by MD for He-Au system with surface temperature 423 K and  $\eta_b = 0.0051$ . Velocities of the beams are normalised by the most probable speed  $\sqrt{2RT}$ . In (c)-(d) MD results are compared against predictions of the SKs for an example case of high impinging velocity of  $\xi'_{t1} = 1.9$  and  $\xi'_{n1} = 1.9$ .

421 cases of small and large reduced densities, similar behaviours are anticipated (e.g., in the  
 422 limit when  $\eta_b$  goes to zero our SK simplifies to the CL model). As expected, the re-emission  
 423 patterns are centred around the line of specular reflection with large tails at small velocities.

424 Figures 5(c-d) show the comparison between the scattering patterns of a monoenergetic  
 425 beam predicted by the different SKs, under a high incident velocity ( $\xi'_{t1} = 1.9$ ,  $\xi'_{n1} = 1.9$ ),  
 426 which is chosen specifically to reveal high deviations from Maxwell's model. It is apparent  
 427 that the tail of the re-emission pattern in the tangential direction is very well captured by our  
 428 SK, while deviations can be clearly seen from the predictions of CL and YTH models. As  
 429 for the normal direction, all the SKs provide satisfactory fits to MD data showing that the  
 430 adsorbate does not affect significantly the scattering dynamics in this direction.

431 Figure 6 shows results similar as in figure 5 but for the He-Au system. Compared to the case  
 432 of argon molecules scattered by a platinum surface, the smaller degree of accommodation to  
 433 the state of the surface makes the tangential distributions narrower near the specular-reflected  
 434 velocity and the tails of the normal distributions thinner. In figure 6(c), a small discrepancy is  
 435 found between the proposed model and the MD result. This is not unexpected since the fine  
 436 details of the real scattering patterns depend on many additional features such as residence  
 437 time, sticking probability and desorption rate, to name a few. Nevertheless, it should be  
 438 emphasised that, despite its simplicity, the proposed model gives an overall good agreement  
 439 with the scattering patterns, as shown in figures 6(c-d), confirming its applicability even  
 440 for gas-surface interactions with intrinsically small momentum and energy accommodations  
 441 (see table 2).

442 A more quantitative comparison of the scattering patterns of monoenergetic beams was  
 443 performed by computing the  $L^2$ -norm errors assuming the MD results as baseline for

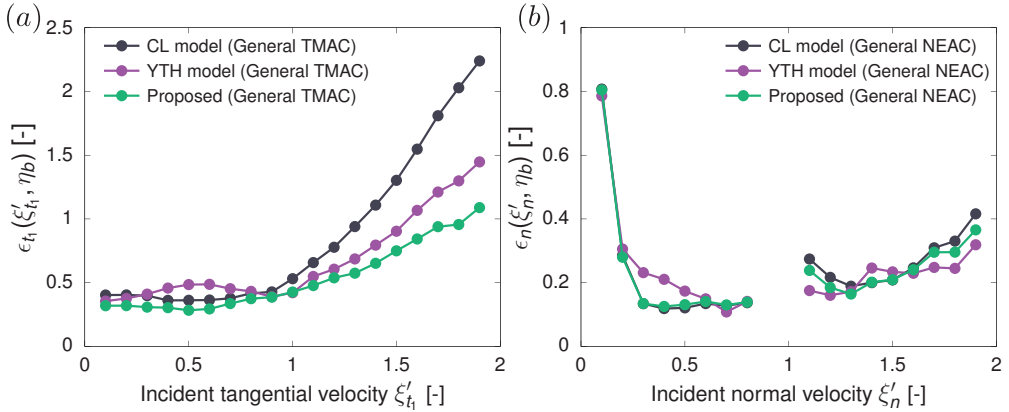


Figure 7: Beam  $L^2$ -norm errors between the reflected velocity distributions of monoenergetic beams predicted by existing SKs and MD results versus the impinging molecule velocity. The results refer to the Ar-Pt system at the surface temperature of 423 K and  $\eta_b = 0.0011$  in the (a) tangential, and (b) normal directions.

444 comparison:

$$445 \quad \epsilon_t(\xi'_t, \eta_b) = \|\mathcal{R}_{\text{SK}}(\xi'_t \rightarrow \xi_t; \eta_b) - \mathcal{R}_{\text{MD}}(\xi'_t \rightarrow \xi_t; \eta_b)\|_2, \quad (5.1a)$$

$$446 \quad \epsilon_n(\xi'_n, \eta_b) = \|\mathcal{R}_{\text{SK}}(\xi'_n \rightarrow \xi_n; \eta_b) - \mathcal{R}_{\text{MD}}(\xi'_n \rightarrow \xi_n; \eta_b)\|_2, \quad (5.1b)$$

448 where

$$449 \quad \|g\|_2 = \left[ \int_{-\infty}^{\infty} g^2 d\xi \right]^{1/2}. \quad (5.1c)$$

450

451 Figure 7 shows the  $L^2$ -norm of the errors of CL, YTH, and our SK for the Ar-Pt system at  
 452 423 K with  $\eta_b = 0.0011$ , and impinging velocities in the range of  $[0, 2]$ . Note that the results  
 453 related to the normal component near the most probable speed have been removed as the  
 454 mathematical definition of ACs is very sensitive to numerical errors in that region (see §2).  
 455 Interestingly, for small velocities, the errors related to the tangential component are almost  
 456 constant, whereas the ones related to the normal component are large. This is likely to be  
 457 attributed to the attractive force field exerted by the surface that is accounted for by none of  
 458 the SKs. Nevertheless, the proposed SK outperforms others in accuracy for both tangential  
 459 and normal scattering patterns.

460 In order to check the accuracy of all SKs over a larger span of reduced densities, the error  
 461 given by (5.1) was integrated with respect to the impinging velocity using the Maxwellian  
 462 flux as a weight, and the results was normalised using the error of the Maxwell fully-diffuse  
 463 model:

$$464 \quad \epsilon_t(\eta_b) = \frac{\int \epsilon_t(\xi'_t, \eta_b) f_0(\xi'_t) d\xi'_t}{\int \|\mathcal{R}_d(\xi_t) - \mathcal{R}_{\text{MD}}(\xi'_t \rightarrow \xi_t)\|_2 f_0(\xi'_t) d\xi'_t}, \quad (5.2a)$$

$$465 \quad \epsilon_n(\eta_b) = \frac{\int_{\xi'_n < 0} \epsilon_n(\xi'_n, \eta_b) f_0(\xi'_n) |\xi'_n| d\xi'_n}{\int_{\xi'_n < 0} \|\mathcal{R}_d(\xi_n) - \mathcal{R}_{\text{MD}}(\xi'_n \rightarrow \xi_n)\|_2 f_0(\xi'_n) |\xi'_n| d\xi'_n}. \quad (5.2b)$$

466

467

468 The error given by (5.2) is computed for the range of reduced densities considered in this  
 469 study, and the results are reported in figures 8(a) and 8(b) for the tangential and normal  
 470 directions, respectively. The proposed SK turns out to be the most accurate. In particular, it

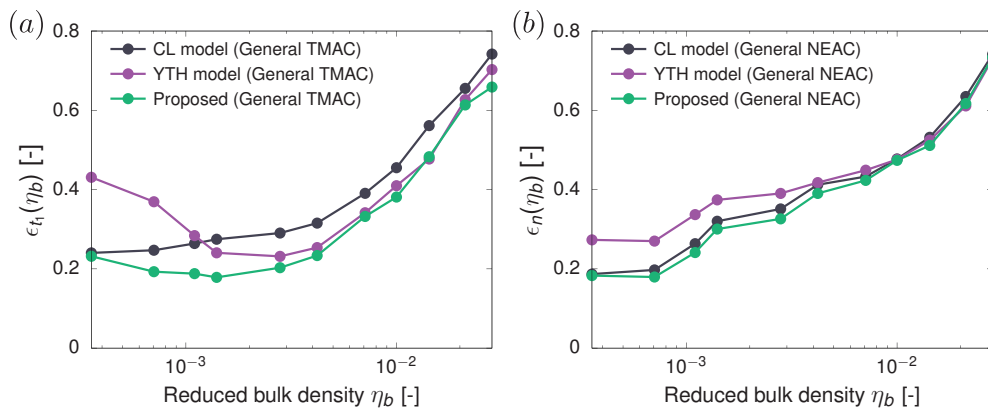


Figure 8: General  $L^2$ -norm errors, obtained by integrating the corresponding beam errors and using the Maxwellian flux as weighted factor, versus the reduced density. The results refer to the Ar-Pt system at the surface temperature of 423 K in the (a) tangential, and (b) normal directions.

471 shows a similar accuracy as the CL model for clean, smooth surfaces (small  $\eta_b$ ), whereas it is  
 472 closer to the YTH model as the degree of adsorption increases (large  $\eta_b$ ). Note that, as already  
 473 pointed out, the adsorbate has a comparatively minor impact on the normal component of the  
 474 scattering patterns and this is clearly reflected by the smaller discrepancies between scattering  
 475 models shown in figure 8(b). Finally, the proposed model is expected to have better overall  
 476 accuracy over existing SKs when considering the He-Au system, where the intrinsic ACs are  
 477 smaller (and the impact of adsorption is found to be more significant) compared to the Ar-Pt  
 478 system.

## 479 6. Concluding remarks

480 Existing scattering kernels (SK) assume that gas molecules impinging on a surface only  
 481 interact with wall atoms, whereas this assumption is inaccurate when an adsorbed layer forms  
 482 next to a surface. In such a condition, gas-gas interactions affect the molecular scattering  
 483 process, as clearly shown by the dependence of the accommodation coefficients (ACs) on  
 484 the gas bulk density. To address this limitation, we have proposed an SK as a simple linear  
 485 combination of the Cercignani-Lampis (CL) and Maxwell fully-diffuse models, using the  
 486 Langmuir isotherm as a weighting factor. The rationale behind our modelling approach is  
 487 that the CL term accurately describes the scattering process from a clean, smooth surface,  
 488 whereas the Maxwell fully-diffuse term is expected to capture also the effect of multiple  
 489 gas-gas interactions when an adsorbed gas layer forms next to the surface. The accuracy of  
 490 various SKs were assessed using high-fidelity Molecular Dynamics (MD) simulations, and  
 491 it was shown that the proposed SK gives the best performance across the range of explored  
 492 bulk densities.

493 Future work will consider the implementation of the proposed scattering model in kinetic  
 494 solvers and to test its performance in heat and flow simulations where adsorption is present.  
 495 The possible extension of the proposed model to polyatomic molecules is also of interest.  
 496 Although there are expressions of the Maxwell fully-diffuse and CL models for this case (Lord  
 497 1991, 1995; Dadzie & Méolans 2004; Hossein Gorji & Jenny 2014) and encouraging results  
 498 in the literature suggesting that a linear combination may work (Yamamoto *et al.* 2007;  
 499 Wu & Struchtrup 2017), a more detailed study using MD is needed to determine whether

500 the coupling between internal and translational energy modes adds complexity and thereby  
501 requiring a more sophisticated modelling approach.

502 **Funding.** This research was funded in whole, or in part, by King Fahd University of Petroleum and Minerals  
503 (KFUPM), Saudi Arabia. M.K.B. and L.G. are funded by the Engineering and Physical Sciences Research  
504 Council (EPSRC) under grant numbers EP/V012002/1, EP/R007438/1. For the purpose of open access, the  
505 author has applied a CC BY public copyright licence to any Author Accepted Manuscript version arising  
506 from this submission.

507 **Declaration of interests.** The authors report no conflict of interest.

## REFERENCES

- 508 AOKI, KAZUO & GIOVANGIGLI, VINCENT 2019 Kinetic model of adsorption on crystal surfaces. *Physical*  
509 *Review E* **99** (5), 052137.
- 510 AOKI, KAZUO & GIOVANGIGLI, VINCENT 2021 Kinetic theory of chemical reactions on crystal surfaces.  
511 *Physica A: Statistical Mechanics and its Applications* **565**, 125573.
- 512 AOKI, KAZUO, GIOVANGIGLI, VINCENT & KOSUGE, SHINGO 2022 Boundary conditions for the boltzmann  
513 equation from gas-surface interaction kinetic models. *Physical Review E* **106** (3), 035306.
- 514 ARKILIC, ERROL B, BREUER, KENNETH S & SCHMIDT, MARTIN A 2001 Mass flow and tangential momentum  
515 accommodation in silicon micromachined channels. *Journal of fluid mechanics* **437**, 29–43.
- 516 ARYA, GAURAV, CHANG, HSUEH-CHIA & MAGINN, EDWARD J 2003 Molecular simulations of knudsen wall-  
517 slip: effect of wall morphology. *Molecular Simulation* **29** (10-11), 697–709.
- 518 BIRD, G. A. 1994a Inelastic collisions and surface interactions. In *Molecular gas dynamics and the direct*  
519 *simulation of gas flows*, pp. 99–122. Oxford University Press.
- 520 BIRD, G. A. 1994b The molecular model. In *Molecular gas dynamics and the direct simulation of gas flows*,  
521 pp. 1–29. Oxford University Press.
- 522 BORMAN, VD, KRYLOV, SU & PROSYANOV, AV 1988 Theory of nonequilibrium phenomena at a gas-solid  
523 interface. *Sov. Phys. JETP* **67** (10), 2110–2121.
- 524 BRANCHER, RICARDO D, STEFANOV, STEFAN, GRAUR, IRINA & FREZZOTTI, ALDO 2020 A kinetic model for  
525 gas adsorption-desorption at solid surfaces under non-equilibrium conditions. *Vacuum* **174**, 109166.
- 526 BRUNAUER, STEPHEN, EMMETT, PAUL HUGH & TELLER, EDWARD 1938 Adsorption of gases in multimolecular  
527 layers. *Journal of the American chemical society* **60** (2), 309–319.
- 528 BUTT, HANS-JÜRGEN, GRAF, KARLHEINZ & KAPPL, MICHAEL 2003 Adsorption. In *Physics and Chemistry of*  
529 *Interfaces*, chap. 9, pp. 177–205. John Wiley & Sons, Ltd.
- 530 CAO, BING-YANG, CHEN, MIN & GUO, ZENG-YUAN 2005 Temperature dependence of the tangential  
531 momentum accommodation coefficient for gases. *Applied Physics Letters* **86** (9), 091905.
- 532 CAO, BING-YANG, SUN, JUN, CHEN, MIN & GUO, ZENG-YUAN 2009 Molecular momentum transport at  
533 fluid-solid interfaces in mems/nems: a review. *International journal of molecular sciences* **10** (11),  
534 4638–4706.
- 535 CERCIGNANI, CARLO 1972 Scattering kernels for gas-surface interactions. *Transport Theory and Statistical*  
536 *Physics* **2** (1), 27–53.
- 537 CERCIGNANI, CARLO 1988 Gas-surface interaction and the h-theorem. In *The Boltzmann equation and its*  
538 *applications*, pp. 104–157. Springer.
- 539 CERCIGNANI, CARLO & LAMPIS, MARIA 1971 Kinetic models for gas-surface interactions. *Transport theory*  
540 *and statistical physics* **1** (2), 101–114.
- 541 CHEN, GANG 2005 *Nanoscale energy transport and conversion: a parallel treatment of electrons, molecules,*  
542 *phonons, and photons*. Oxford university press.
- 543 CHEN, YICHONG, LI, JUN, DATTA, SAIKAT, DOCHERTY, STEPHANIE Y, GIBELLI, LIVIO & BORG, MATTHEW K  
544 2022 Methane scattering on porous kerogen surfaces and its impact on mesopore transport in shale.  
545 *Fuel* **316**, 123259.
- 546 CHEW, AD 2009 Comment on “survey on measurement of tangential momentum accommodation  
547 coefficient”[j. vac. sci. technol. a 26, 634 (2008)]. *Journal of Vacuum Science & Technology A:*  
548 *Vacuum, Surfaces, and Films* **27** (3), 591–592.
- 549 COWLING, TG 1974 On the cercignani-lampis formula for gas-surface interactions. *Journal of Physics D:*  
550 *Applied Physics* **7** (6), 781.

- 551 DADZIE, S KOKOU & MÉOLANS, J GILBERT 2004 Anisotropic scattering kernel: Generalized and modified  
552 maxwell boundary conditions. *Journal of Mathematical Physics* **45** (5), 1804–1819.
- 553 EPSTEIN, MELVIN 1967 A model of the wall boundary condition in kinetic theory. *AIAA Journal* **5** (10),  
554 1797–1800.
- 555 FINGER, GEORGE W, KAPAT, JAYANTA S & BHATTACHARYA, ANIKET 2007 Molecular dynamics simulation  
556 of adsorbent layer effect on tangential momentum accommodation coefficient .
- 557 FREUNDLICH, HERBERT 1922 *Kapillarchemie: eine Darstellung der Chemie der Kolloide und verwandter*  
558 *Gebiete*. akademische Verlagsgesellschaft.
- 559 GOODMAN, FRANK O 1974 Thermal accommodation. *Progress in Surface Science* **5**, 261–375.
- 560 GOODMAN, FRANK O. & WACHMAN, HAROLD Y. 1976a Chapter 5 - molecular beams. In *Dynamics of*  
561 *Gas-Surface Scattering* (ed. Frank O. Goodman & Harold Y. Wachman), pp. 73–102. Academic  
562 Press.
- 563 GOODMAN, FRANK O. & WACHMAN, HAROLD Y. 1976b Chapter 8 - quantum theory of gas–surface scattering.  
564 In *Dynamics of Gas-Surface Scattering* (ed. Frank O. Goodman & Harold Y. Wachman), pp. 143–180.  
565 Academic Press.
- 566 HOSSEIN GORJI, M & JENNY, PATRICK 2014 A gas-surface interaction kernel for diatomic rarefied gas flows  
567 based on the cercignani-lampis-lord model. *Physics of fluids* **26** (12), 122004.
- 568 KLINC, TOMAŽ & KUŠČER, IVAN 1972 Slip coefficients for general gas-surface interaction. *The Physics of*  
569 *Fluids* **15** (6), 1018–1022.
- 570 KUŠČER, IVAN 1971 Reciprocity in scattering of gas molecules by surfaces. *Surface Science* **25** (2), 225–237.
- 571 KUŠČER, IVAN 1978 Phenomenological aspects of gas-surface interaction. In *Fundamental Problems in*  
572 *Statistical Mechanics IV* (ed. E.G.D. Cohen & W. Fiszdon), pp. 441–467. Ossolineum, Warsaw.
- 573 KUŠČER, IVAN 1974 Phenomenology of gas-surface accommodation. In *Rarefied Gas Dynamics, Proceeding*  
574 *of the Ninth International Symposium* (ed. M Becker & M Fiebig), pp. E.1–1–21. DFVLR-Press,  
575 Porz-Wahn, Germany.
- 576 KUŠČER, IVAN, MOZINA, J & KRIZAMIČ, F 1971 In *Rarefied Gas Dynamics, Proceeding of the Seventh*  
577 *International Symposium* (ed. Silvio Nocilla Dino Dini, Carlo Cercignani), p. 97. Edizioni Tecnico  
578 Scientifica, Pisa.
- 579 LANGMUIR, IRVING 1916 The constitution and fundamental properties of solids and liquids. part i. solids.  
580 *Journal of the American chemical society* **38** (11), 2221–2295.
- 581 LIAO, MENG, GRENIER, ROMAIN, TO, QUY-DONG, DE LARA-CASTELLS, MARÍA PILAR & LEONARD, CELINE  
582 2018 Helium and argon interactions with gold surfaces: Ab initio-assisted determination of the he–au  
583 pairwise potential and its application to accommodation coefficient determination. *The Journal of*  
584 *Physical Chemistry C* **122** (26), 14606–14614.
- 585 LIVADIOTTI, SABRINA, CRISP, NICHOLAS H, ROBERTS, PETER CE, WORRALL, STEPHEN D, OIKO, VITOR TA,  
586 EDMONDSON, STEVE, HAIGH, SARAH J, HUYTON, CLAIRE, SMITH, KATHARINE L, SINPETRU, LUCIANA A  
587 & OTHERS 2020 A review of gas-surface interaction models for orbital aerodynamics applications.  
588 *Progress in Aerospace Sciences* **119**, 100675.
- 589 LORD, RG 1991 Some extensions to the cercignani–lampis gas–surface scattering kernel. *Physics of Fluids*  
590 *A: Fluid Dynamics* **3** (4), 706–710.
- 591 LORD, RG 1995 Some further extensions of the cercignani–lampis gas–surface interaction model. *Physics*  
592 *of Fluids* **7** (5), 1159–1161.
- 593 MAXWELL, JAMES CLERK 1879 Vii. on stresses in rarified gases arising from inequalities of temperature.  
594 *Philosophical Transactions of the royal society of London* (170), 231–256.
- 595 MYONG, RS 2004 Gaseous slip models based on the langmuir adsorption isotherm. *Physics of fluids* **16** (1),  
596 104–117.
- 597 NEJAD, SHAHIN MOHAMMAD, NEDEA, SILVIA, FRIJNS, ARJAN & SMEULDERS, DAVID 2020 The influence of  
598 gas–wall and gas–gas interactions on the accommodation coefficients for rarefied gases: A molecular  
599 dynamics study. *Micromachines* **11** (3), 319.
- 600 PILINSKI, MARCIN D, ARGROW, BRIAN M, PALO, SCOTT E & BOWMAN, BRUCE R 2013 Semi-empirical  
601 satellite accommodation model for spherical and randomly tumbling objects. *Journal of Spacecraft*  
602 *and Rockets* **50** (3), 556–571.
- 603 PLIMPTON, STEVE 1995 Fast parallel algorithms for short-range molecular dynamics. *Journal of*  
604 *computational physics* **117** (1), 1–19.
- 605 RETTNER, CT, SCHWEIZER, EK & MULLINS, CB 1989 Desorption and trapping of argon at a 2h–w (100)  
606 surface and a test of the applicability of detailed balance to a nonequilibrium system. *The Journal of*  
607 *Chemical Physics* **90** (7), 3800–3813.

- 608 SAZHIN, OLEG V, BORISOV, SERGEI F & SHARIPOV, FELIX 2001 Accommodation coefficient of tangential  
609 momentum on atomically clean and contaminated surfaces. *Journal of Vacuum Science & Technology*  
610 *A: Vacuum, Surfaces, and Films* **19** (5), 2499–2503.
- 611 SHAN, BAOCHAO, WANG, PENG, WANG, RUNXI, ZHANG, YONGHAO & GUO, ZHAOLI 2022 Molecular kinetic  
612 modelling of nanoscale slip flow using a continuum approach. *Journal of Fluid Mechanics* **939**.
- 613 SHARIPOV, FELIX 2002 Application of the cercignani–lampis scattering kernel to calculations of rarefied gas  
614 flows. i. plane flow between two parallel plates. *European Journal of Mechanics-B/Fluids* **21** (1),  
615 113–123.
- 616 SPIJKER, PETER, MARKVOORT, ALBERT J, NEDEA, SILVIA V & HILBERS, PETER AJ 2010 Computation of  
617 accommodation coefficients and the use of velocity correlation profiles in molecular dynamics  
618 simulations. *Physical Review E* **81** (1), 011203.
- 619 STRUCHTRUP, HENNING 2013 Maxwell boundary condition and velocity dependent accommodation  
620 coefficient. *Physics of Fluids* **25** (11), 112001.
- 621 TAKATA, SHIGERU, AKASOBE, SHIGENORI & HATTORI, MASANARI 2021 A revisit to the cercignani–lampis  
622 model: Langevin picture and its numerical simulation. In *Recent Advances in Kinetic Equations and*  
623 *Applications*, pp. 345–365. Springer.
- 624 WANG, RUNXI, LI, JUN, GIBELLI, LIVIO, GUO, ZHAOLI & BORG, MATTHEW K 2021 Sub-nanometre pore  
625 adsorption of methane in kerogen. *Chemical Engineering Journal* **426**, 130984.
- 626 WILLIAMS, MMR 1971 A phenomenological study of gas-surface interactions. *Journal of Physics D: Applied*  
627 *Physics* **4** (9), 1315.
- 628 WU, LEI & STRUCHTRUP, HENNING 2017 Assessment and development of the gas kinetic boundary condition  
629 for the boltzmann equation. *Journal of Fluid Mechanics* **823**, 511–537.
- 630 YAKUNCHIKOV, AN, KOVALEV, VL & UTYUZHNIKOV, SV 2012 Analysis of gas-surface scattering models  
631 based on computational molecular dynamics. *Chemical Physics Letters* **554**, 225–230.
- 632 YAMAMOTO, KYOJI, TAKEUCHI, HIDEKI & HYAKUTAKE, TORU 2006 Characteristics of reflected gas molecules  
633 at a solid surface. *Physics of Fluids* **18** (4), 046103.
- 634 YAMAMOTO, KYOJI, TAKEUCHI, HIDEKI & HYAKUTAKE, TORU 2007 Scattering properties and scattering  
635 kernel based on the molecular dynamics analysis of gas-wall interaction. *Physics of Fluids* **19** (8),  
636 087102.